NASA TECHNICAL MEMORANDUM

NASA TM X-62,092

NASA TM X-62,092

ARC JET TESTS OF METALLIC TPS MATERIALS

Frank J. Centolanzi, Hubert B. Probst, Carl E. Lowell,
and Norman B. Zimmerman

Ames Research Center
Moffett Field, Calif., 94035
and
Lewis Research Center
Cleveland, Ohio, 44135

October 1971

Technical paper presented at the Space Shuttle Materials Conference, Huntsville, Alabama, October 5-7, 1971, sponsored by the Society of Aerospace Material and Process Engineers

ARC JET TESTS OF METALLIC TPS MATERIALS

By Frank J. Centolanzi,* Hubert B. Probst,**
Carl E. Lowell,** and Norman B. Zimmerman*

ABSTRACT

Seven thoria dispersed nickel base alloys and one cobalt base alloy, candidates for the Metallic Thermal Protection System for the Space Shuttle Vehicle, were tested simultaneously in an arc jet at a nominal test temperature of 1366°K (2000°F) and pressure of 0.01 atmospheres. The degradation of the materials after 50 one half-hour cycles in the arc jet simulating Space Shuttle entry conditions was determined utilizing techniques including X-ray diffraction, metallography, and electron beam microprobe.

INTRODUCTION

Metallic thermal protection systems are receiving widespread attention for use on the space shuttle vehicle. The heat shields on this vehicle are intended for repeated reuse without refurbishment; therefore, they must be resistant to oxidation at high temperatures for relatively long times. Most of the work directed toward determining the oxidation resistance of these alloys has been done in a static environment, that is, no flow over the surface (Ref. 1). A velocity effect on corrosion rates has been noted (Ref. 2, 3 and 4) and it was shown in Ref. 5 that a hypervelocity air stream was necessary to simulate adequately the oxidation of thoria dispersed nickel chromium alloys in flight. A theoretical model describing the oxidation and weight removing mechanisms for thoria dispersed nickel chromium alloys was developed in Ref. 6, and the predictions were compared with the experimental results of Ref. 4 and 5.

The present paper reports the results of tests with eight different alloys developing oxides at different rates with attendant differences in specimen temperature resulting from differences in emissivity and possibly even surface catalytic effects. This would, however, be the case in flight and is an appropriate means for direct comparison of competing materials for a given heating rate range on the vehicle surface. In this investigation the eight metallic alloys were simultaneously exposed to an arc-heated hypervelocity air stream for 50 cycles of 30 minute duration. The nominal test temperature was 1366°K (2000°F) and the surface pressure 1000 N/M^2 (0.01 atm). The eight metallic

*Ames Research Center, NASA, Moffett Field, California 94035
**Lewis Research Center, NASA, Cleveland, Ohio 44135

alloys investigated were: TD-Ni-20Cr; DS-Ni-20Cr; TD-Ni-20Cr-15Fe; TD-Ni-16Cr-(X)Al-0.4Y (x > 3.5, Proprietary); TD-Ni-16Cr-3.5Al; TD-Ni-20Cr-3.5Al; TD-Ni; and HS-188.

The preliminary results of this investigation were reported in Ref. 7. After exposure to simulated flight conditions, the specimens were analyzed at the NASA-Lewis Research Center. This metallurgical investigation consisted of X-ray diffraction, metallography, metal thickness change, and electron beam microprobe measurements. A comparison of the relative performance of these alloys is made and factors which affect their reuse are discussed.

APPARATUS

Arc-Jet Facility

The tests were conducted in the Ames Entry Aerodynamic Facility of the Thermal Protection Branch. This facility is designed to accommodate a variety of arc heaters and nozzle combinations thereby providing a wide range of test conditions. For these tests, a commercially available unit, a Linde N4001 heater with a 1 inch diameter throat was used. The basic heater is described in Ref. 8. The vacuum system used with the arcs is a continuous multi-stage steam ejector type capable of pressures down to 50 microns at mass flows of 0.4 lb/sec. The arcs can operate at powers to 5 MW at pressures to 700 psia. A typical arc heater set up is shown in Fig. 1.

Multiple Sample Support

The multiple-sample stagnation test support used for these tests is shown in Fig. 2. This copper, water-cooled support accommodates eight samples 4.45 cm (1.75 in.) in diameter. Each sample is backed by a low-density silica insulating material to reduce the heat loss to the support. A platinum-platinum, 13-percent rhodium thermocouple was spotwelded to the rear of each specimen. A steady-state calorimeter mounted at the center, and pressure orifices distributed across the face of the support provided direct measurements of heating rate and pressure during the test. A photograph of the support mounted in the test chamber is shown in Fig. 3. A 61 cm (24 in.) nozzle used for these tests can also be seen in this photograph together with the pitot probe and hemispherical calorimeter used to measure the pressure and determine the enthalpy of the steam.

TEST SPECIMENS

A typical fabricated test specimen is shown in Fig. 2b. In general the specimens were fabricated in one piece including the support tabs. Two of the alloys (TD-Ni-16Cr-(X)Al-0.4Y and TD-Ni-20Cr-3.5Al) could not be bent to the small radius required for the support tabs. For these specimens TD-Ni-20Cr tabs were spot welded to the flat circular disk. In all cases the as-received surface condition was maintained. The specimens were not pre-oxidized prior to arc-jet exposure.

The alloys tested are listed below.

Material	Nominal Thickness mm	inches
TD-Ni-20Cr*	.269	.0106
DS-Ni-20Cr	.280	.0110
TD-Ni-20Cr-15Fe	.346	.0136
TD-Ni-16Cr-(X)Al-0.4Y (x > 3.5, proprietary)	.285	.0112
TD-Ni-16Cr-3.5Al	.394	.0155
TD-Ni-20Cr-3.5Al	.407	.0160
TD-Ni	.531	.0209
HS-188	.437	.0172

*Weight Percent
TD(Thoria dispersed)
DS(Dispersion strengthened)

All TD alloys were obtained from Fansteel Inc. The DS alloy is made by Sherritt-Gordon Mines Ltd. by a process different from that used for TD alloys, although DS is also strengthened by dispersed thoria. HS-188 is a cobalt-base superalloy from the Stellite Division of the Cabot Corporation.

INSTRUMENTATION

The specimen temperature, pressure, and heating rate were recorded continuously during the tests using a recording oscillograph. The millivolt output of the thermocouples was also monitored using a digital voltmeter. Specimen temperatures were also measured with a disappearing-filament optical pyrometer ($\lambda = 0.65\ \mu$) during the tests.

The stream enthalpy was determined using a transient-type hemispherical calorimeter 3.17 cm (1.25 in.) in diameter, and the centerline impact pressure was measured using a conventional pitot probe.

TESTS

The nozzle and arc heater configuration for these tests provided a supersonic test stream with a Mach number of approximately six for which pressure and enthalpy could be varied during the test. The nominal specimen temperatures and surface pressures for these tests were 1366°K (2000°F) and 1000 N/M^2 (0.01 atm), respectively. However, since the emissivities of the test specimens changed considerably during the first few cycles, it was necessary to vary the heating rates initially to avoid excessive specimen temperatures until a stable oxide was formed. A typical test cycle consisted of inserting the specimens into the arc-heated stream for 30 minutes and then removing them from the stream to cool. After visual inspection of the specimens, this procedure was repeated. A photograph taken during a typical run is shown in Fig. 4. The front face of the support, and the hot specimens can be seen reflected by the mirror located at the left. After 50 cycles were completed in this fashion the tests were terminated. The specimens were photographed before disassembly of the support system and are shown in Fig. 5. After disassembly the spot welded thermocouple beads were cut flush to the specimen surface and post run weights measured. The specimens were then analyzed metallurgically at the NASA-Lewis Research Center.

TEST RESULTS

Heating Rate and Temperature Histories

The nominal stagnation temperature for these tests was 1366°K (2000°F). The equilibrium temperatures of the test specimens however, are dependent upon heating rate and emissivity. Since the emissivity was different for each material, and also varied with time as the specimens developed their equilibrium oxide coating, it was impossible to perform the tests at a constant surface temperature. The heating rates during the first twenty test cycles were dictated by the response of two of the thoriated alloys containing aluminum. After equilibrium temperatures were reached the heating rates were held constant. The resulting heating rate, enthalpy, and temperature histories are shown in Figs. 6 to 8.

For radiation-equilibrium heat transfer the heating rate and temperature are related by the expression

$$q = \epsilon \sigma T_w^4$$

where T_w is the specimen wall temperature, q the heating rate, ϵ the emissivity, and σ the Stefan-Boltzmann constant. For constant emissivity, the temperature and heating-rate profiles should have the same general shape. The temperature histories for the two alloys, TD-Ni-16Cr-(X)Al-0.4Y and TD-Ni-16Cr-3.5Al are characteristically different than the others. There is an initial increase of temperature with exposure followed by a decrease. This indicates the emissivity is increasing slowly with time of exposure after peak temperature has been reached. These two alloys, which are highly oxidation resistant, require longer times to develop their stable oxide coatings. This observed variation of emissivity with time serves to emphasize the need for preoxidation before heat shields of these materials are used for flight application.

Weight Changes

At the conclusion of 50 cycles of exposure the specimens were removed from the support, thermocouples removed, and the samples weighed. The total weight changes per unit frontal area are shown in Table I.

The alloys TD-Ni-20Cr, DS-Ni-20Cr, TD-Ni-20Cr-15Fe, and TD-Ni-20Cr-3.5Al all lost about the same amount of weight. The mass loss for the TD-Ni-20Cr alloys are consistent with those reported in Ref. 5. The HS-188 specimen lost more weight than any of the materials tested. The oxide layer for this specimen was very powdery and could be easily wiped off. In contrast to the other specimens, the TD-Ni specimen experienced a relatively large weight gain. The aluminum bearing alloys TD-Ni-16Cr-(X)Al-0.4Y and TD-Ni-16Cr-3.5Al showed the smallest change in weight.

METALLURGICAL INVESTIGATION

After arc-jet exposure, the oxide phases present in the surface scale, and their relative abundances, were determined by X-ray diffraction. The specimens were then mounted in epoxy and sectioned along the original mill rolling directions through the diameter. The HS-188 specimen was not cut along the rolling direction since its direction was not known. After sectioning, the specimens were polished, ultrasonically cleaned, and the residual metal thickness measured with a filar eyepiece mounted on a microscope. Photomicrographs were taken of each specimen. The specimens were then acid etched and photographed again. The primary etch used was 100 ml H_2O, 2 gms chromic acid, and 10 ml H_2SO_4, electrolytic. This was used in all cases except TD-Ni for which the etch was 92 HCL, $3HNO_3$ and $5H_2SO_4$. The unetched photographs were used to evaluate porosity and etching was used to bring out the microstructure and visually show chromium depletion. Only the photomicrographs

of the etched specimens are shown in this paper. Finally, the specimens (except TD-Ni) were subjected to microprobe analysis across the thickness primarily to determine chromium depletion. The microprobe used for this investigation was capable of scanning three elements simultaneously. The scans were made near the center of the samples in all cases. For HS-188, which contains six elements of interest, more than one scan was needed. The metallurgical results are discussed in the following sections and summarized in Table I.

Metal Thickness Loss

The average metal thickness loss for all the specimens tested is shown in Table I. With the exception of TD-Ni and HS-188 the average metal losses are nearly equal. In fact, the variation in metal loss on some individual specimens was found to be larger than the differences among specimens. TD-Ni had the highest metal loss of any of the materials tested (0.056 mm) (0.0022 in.). HS-188 was second highest (0.038 mm) (0.0015 in.), despite the fact its temperature was the lowest.

Surface-Scale Identification

The oxides found in the surface scale by X-ray diffraction are listed in Table I. It should be noted that relative strengths are subject to many sources of error. The composition of the spinels could not be determined by the diffraction data alone, but are inferred from alloy composition and microprobe data.

MICROPROBE DATA AND MICROSTRUCTURES

The microprobe scans and photomicrographs for all the specimens are shown in Figs. 9 to 17 and discussed in the following paragraphs.

TD-Ni-20Cr, DS-Ni-20Cr and TD-Ni-20Cr-15Fe

The microprobe results and microstructures for these alloys are shown in Fig. 9 to 12. In general, the chromium profiles are the same. The depths of depletion varied from 0.110 to 0.140 mm and the chromium concentration at the metal oxide interface drops to about one half the value in the unaffected zone. The TD-Ni-20Cr-15Fe sample may have slightly more chromium depletion on the backside, but the difference is slight. The electron probe traces indicate a large number of Cr_2O_3 particles throughout the TD-Ni-20Cr-15Fe sample as suggested by the locally increased Cr concentrations. There are fewer such particles in TD-Ni-20Cr. No indication of such particles was found in DS-Ni-20Cr which is probably due to the different processing steps.

The microstructures of TD-Ni-20Cr and TD-Ni-20Cr-15Fe were similar. Both had extensive porosity and chromium depletion, especially on the side exposed to the air stream. DS-Ni-20Cr, in contrast, developed only a few isolated voids near the surface. However, DS-Ni-20Cr showed about the same amount of chromium depletion when etched and, in addition, had the "wormy" structure generally seen in this material and associated with ThO_2 depleted zones. In order to determine if very small pores were being developed, electron micrographs were made (Fig. 11). No pores were found but the presence of ThO_2 free zones was confirmed.

TD-Ni-16Cr-(X)Al-0.4Y, TD-Ni-16Cr-3.5Al, and TD-Ni-20Cr-3.5Al

For these alloys, all of the microprobe traces were similar (Figs. 13 to 15). There was no evidence of appreciable chromium or aluminum depletion, and all showed high aluminum in the scale. Confirmation that the particles contained within the alloys were Al_2O_3 was apparent from the aluminum spikes on the traces which correspond to low chromium and nickel regions.

The photomicrographs for the three samples are similar except for one important exception. All but TD-Ni-20Cr-3.5Al which formed a spinel, had an oxide layer which was dense and tightly adherent. In contrast, TD-Ni-20Cr-3.5Al, had a poorly bonded, poorly adherent, duplex layered oxide (Fig. 15).

HS-188

The microprobe scans and photomicrograph for HS-188 are shown in Fig. 16. Silica and chromium are depleted to a depth of about 0.050 MM. The silicon is concentrated to a great degree at the scale-metal interface indicating the possibility of an SiO_2 layer, although none was found by X-ray diffraction. This may indicate that any SiO_2 present is amorphous. The microstructure indicates some internal oxidation and/or surface region porosity, and a duplex, cracked scale.

TD-Ni

No microprobe scans were made on this material. The microstructure (Fig. 17) reveals a thick NiO layer and a few inclusions in the metal.

CONCLUDING REMARKS

A number of candidate thermal protection system metal alloy samples were tested at conditions [nominal temperature 1366°K (2000°F) and surface pressure

1000 N/M^2 (0.01 atm)] that simulate some entry conditions for the space shuttle vehicle and analysis of the test results lead to the following remarks:

The HS-188 and TD-Ni specimens were the least oxidation resistant as judged by metal thickness loss criterion, even though the TD-Ni gained weight while the HS-188 lost weight. In addition, HS-188 showed marked alloy depletion.

The other specimens tested all lost small and comparable amounts of metal thickness. Chromium depletion was extensive in TD-Ni-20Cr, TD-Ni-20Cr-15Fe, and DS-NI-20Cr, and considerable porosity developed in TD-Ni-20Cr and TD-Ni-20Cr-15Fe but none was evident in DS-Ni-20Cr. In contrast to the thoriated alloys without aluminum, those with aluminum showed neither alloy depletion zones nor porosity. The thoriated alloys containing aluminum were therefore rated the best performers as a group. Within this group, TD-Ni-20Cr-3.5Al appeared to have a greater tendency to spall, and hence, was less oxidation resistant. This conclusion should be qualified, however, with the knowledge that the TD-Ni-20Cr-3.5Al specimen had the highest surface temperature of any alloy during the tests.

The source of the porosity in TD-Ni-20Cr and TD-Ni-20Cr-15Fe has usually been explained as due to the formation of Kirkendall voids. However, it is not clear why such voids do not form in DS-Ni-20Cr. A possible explanation is that the voids are nucleated by Cr_2O_3 particles which are present in the TD alloys containing chromium, but not in DS-Ni-20Cr. This is still under investigation.

Ultimately, the effect of oxidation must be judged by its influence on the mechanical properties of the alloys. While this is beyond the scope of the present report, some speculation may be made. The void formation and chromium depletion is unlikely to be beneficial. It is therefore likely that the mechanical properties of thoriated alloys containing aluminum will be affected less by exposure to aerodynamic heating than those of the other alloys tested. Thus, it appears that such alloys hold more potential for the TPS application than do thoriated nickel chromium alloys without aluminum.

Several problems of analysis arise from simultaneously testing competing Thermal Protection System alloys at the same aerodynamic heating rates. There were variations in specimen surface temperatures resulting from differences in emissivity and possibly surface catalytic effects. The effect of these variations in material test temperatures is difficult to evaluate unless further information is available concerning the temperature dependence of the oxidation on the alloys.

REFERENCES

1. Sanders, W. A., and Barrett, C. A.: Oxidation Screening at 1204°C (2200°F) of Candidat Alloys for the Space Shuttle Thermal Protection System. NASA TMX-67864.

2. Probst, Hubert B.: Effect of Environment on Erosion-Corrosion Processes. Aerospace Structural Materials. NASA SP-227, 1970, pp. 279-293.

3. Sanders, W. A., and Probst, H. B.: Hot Corrosion of TD-Nickel and TD-Nickel Chromium in a High Velocity Gas Stream. NASA TMX-52, 976. May 1971.

4. Johnston, R., and Ashbrook, R. L.: Oxidation and Thermal Fatigue Cracking of Nickel and Cobalt-Base Alloys in a High Velocity Gas Stream. NASA TND-5376, August 1969.

5. Centolanzi, F. J.: Hypervelocity Oxidation Tests of Thoria Dispersed Nickel Chromium Alloys. NASA TMX-62,015. (SSPD-28).

6. Goldstein, Howard E.: An Analytical Model for Hypersonic Ablation of Thoria Dispersed Nickel Chromium Alloy. Paper presented at AIAA 9th Aerospace Sciences Meeting, New York, January 25-27, 1971. Also available as SSPD-23.

7. Larson, Howard K., Centolanzi, Frank J., Vojvodich, Nick S., Goldstein, Howard E., Covington, M. Alan, and Matting, Fred W.: Environmental Testing for Evaluation of Space Shuttle Thermal Protection Materials and Systems. NASA TMX-2273.

8. Sarlitto, R. J. et al., Development of High Enthalpy, High P Arc Air Heaters, RTD-TDR-63-4055, Feb. 1964, Aeronautical Syste v., Wright-Patterson Air Force Base, Ohio.

TABLE I - SUMMARY OF RESULTS

MATERIAL	STEADY STATE TEMPERATURE, °K(°F)	WEIGHT CHANGE, mg/cm^2	METAL THICKNESS LOSS, mm(in.)	DEPTH OF POROSITY, mm(in.)	DEPTH OF Cr DEPLETION, mm(in.)	SCALE IDENTIFICATION	
						OXIDE	RELATIVE STRENGTH*
TD-Ni-20Cr	1411 (2080)	-2.1	0.018 (0.0007)	0.135 (0.005)	0.10 (0.004)	Cr_2O_3	M
						SPINEL ($NiCr_2O_4$)	W
DS-Ni-20Cr	1405 (2070)	-3.5	0.015 (0.0006)	Very Little	0.13 (0.005)	Cr_2O_3	M
						SPINEL ($NiCr_2O_4$)	M
TD-Ni-20Cr-15Fe	1402 (2065)	-2.1	0.023 (0.0009)	0.115 (0.004)	0.15 (0.006)	SPINEL ($NiCr_2O_4$ + Fe)	S
						Cr_2O_3	M
TD-Ni-16Cr-(x)Al-0.4Y Proprietary x>3.5	1377 (2020)	0.7	0.018 (0.0007)	None	0	Al_2O_3	S
TD-Ni-16Cr-3.5Al	1400 (2060)	0.2	0.015 (0.0006)	None	0	Al_2O_3	S
TD-Ni-20Cr-3.5Al	1455 (2160)	-3.1	0.020 (0.0008)	None	0	Al_2O_3	S
						SPINEL ($NiAl_2O_4$)	M
TD-Ni	1433 (2120)	8.4	0.056 (0.0022)	None	No Cr Present	NiO	S
HS-188	1377 (2020)	-7.5	0.038 (0.0015)	Restricted To Surface	0.05 (0.002)	SPINEL ($CoCr_2O_4$+Mn)	S
						Cr_2O_3	M

* S-strong, M-medium, W-weak

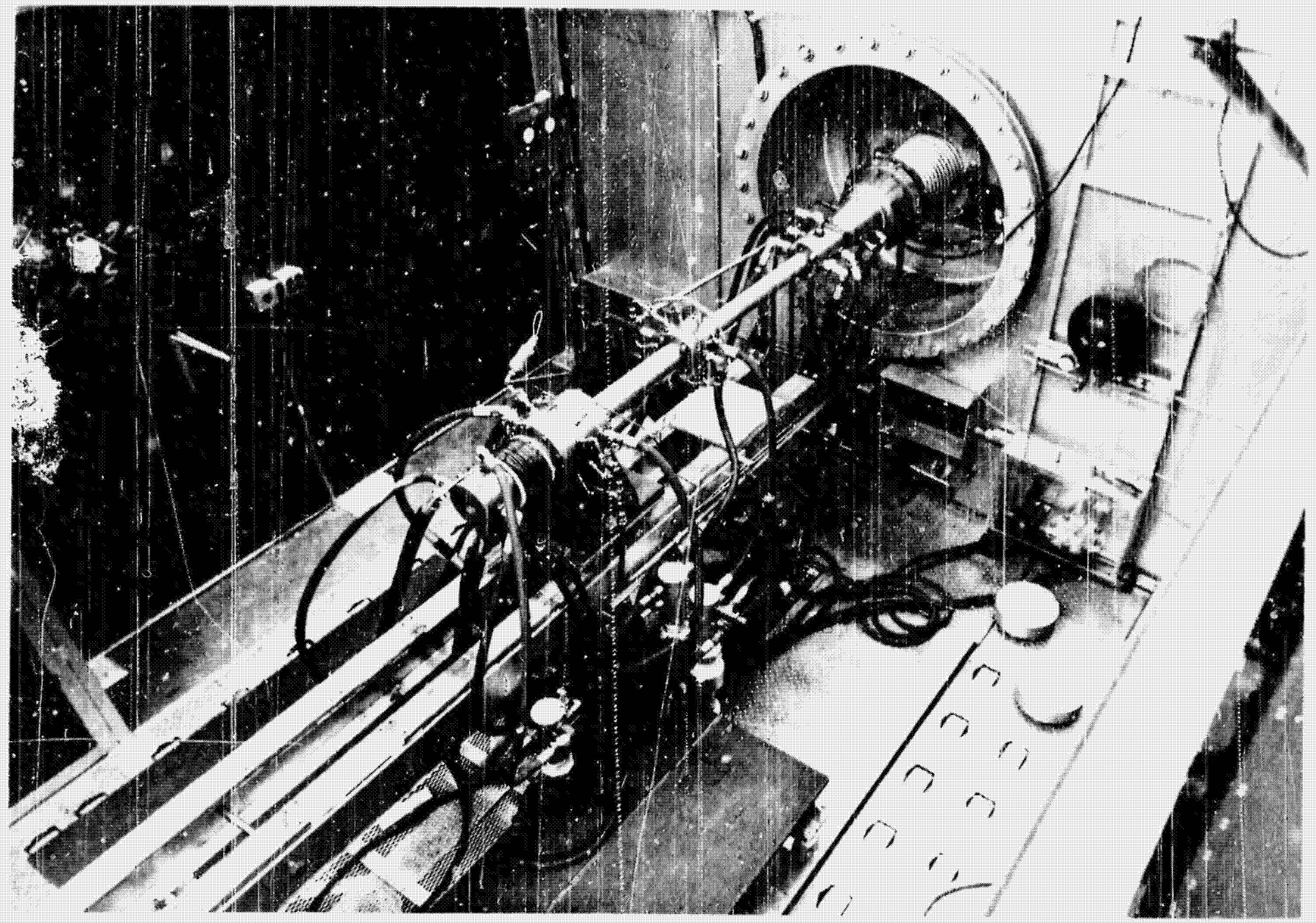

Fig. 1.- Arc heater setup.

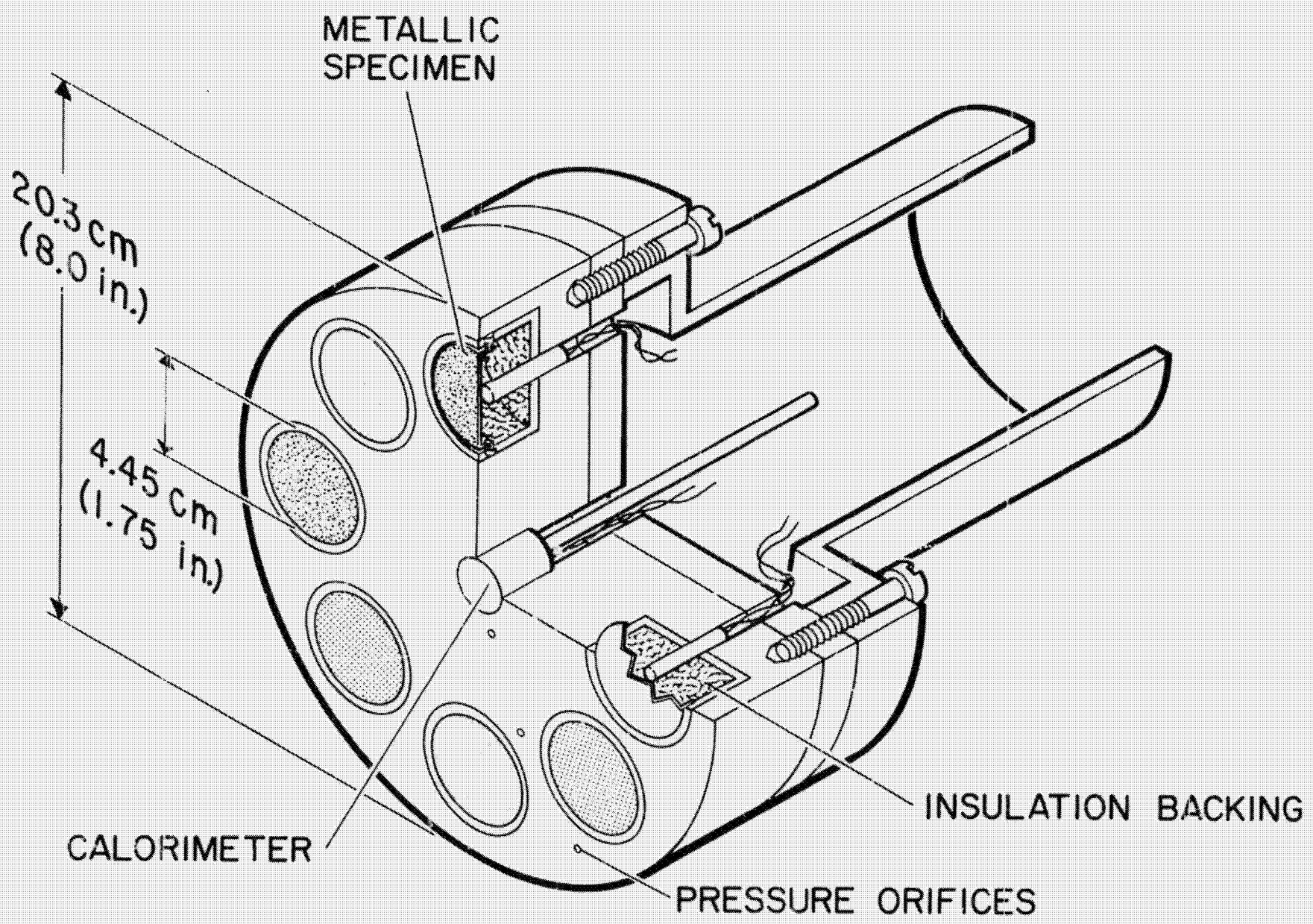

(a) Schematic drawing.

Fig. 2.- Multiple sample stagnation support.

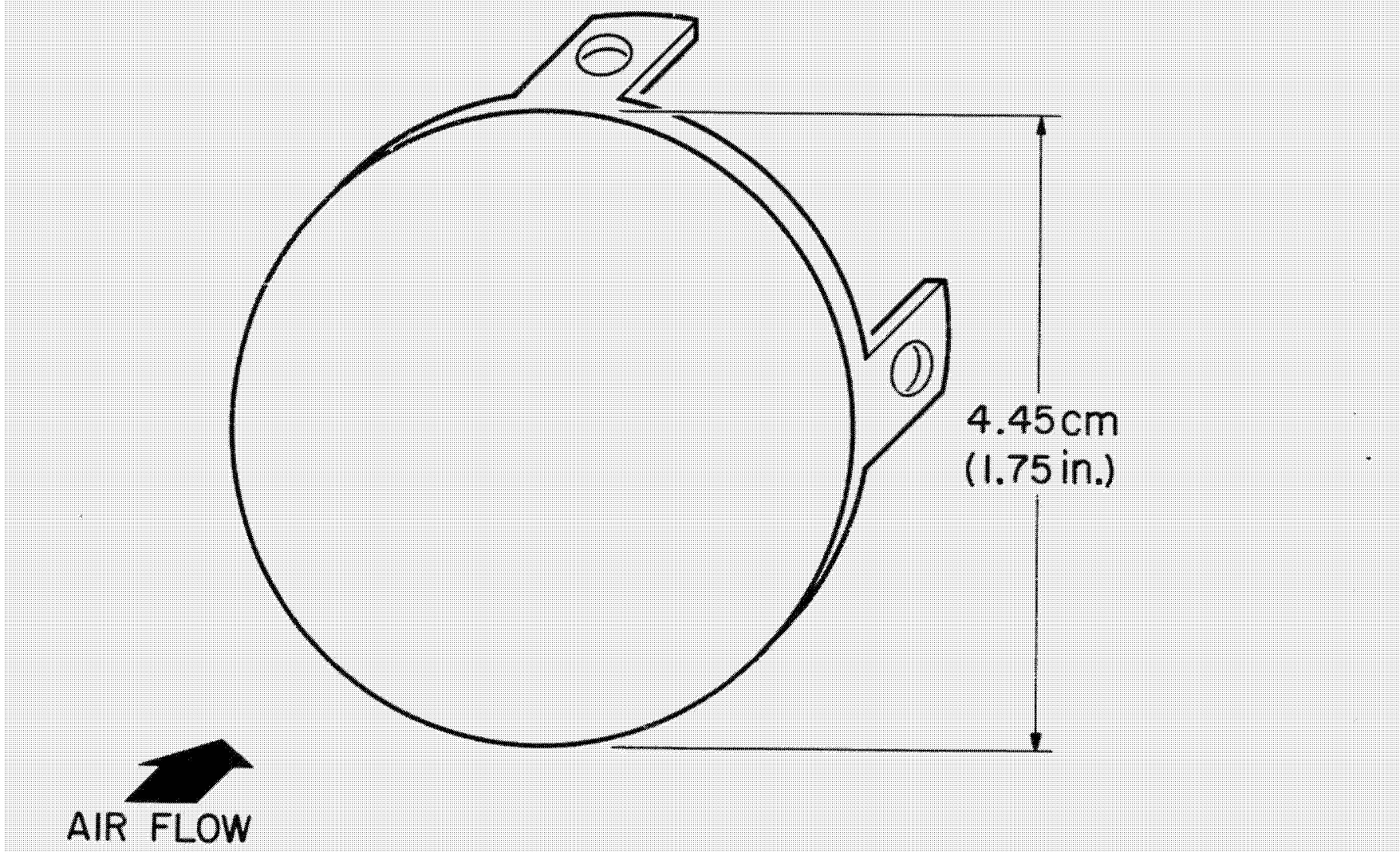

(b) Test specimen detail.

Fig. 2.- Continued.

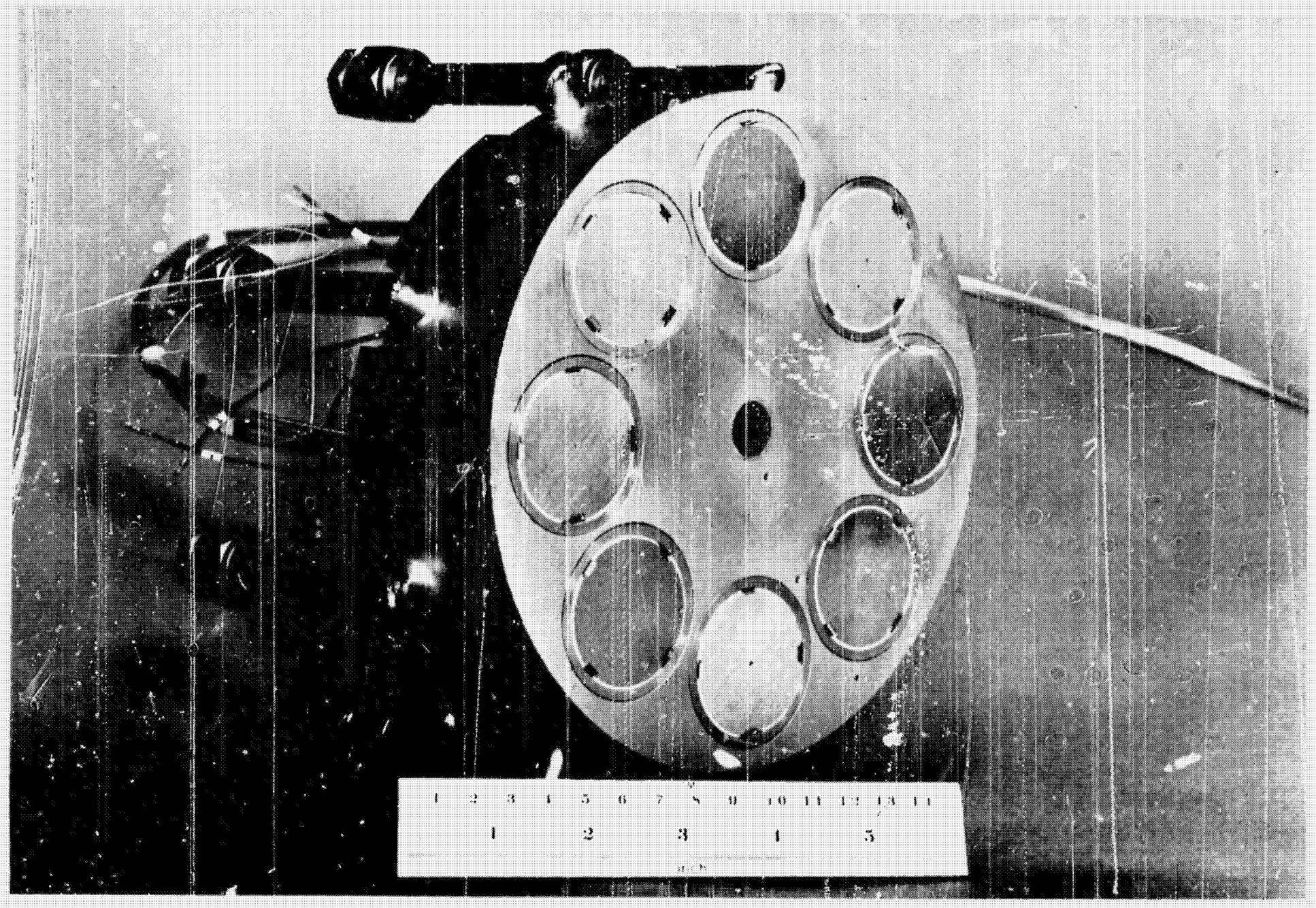

(c) Photograph taken before test.

Fig. 2.- Concluded.

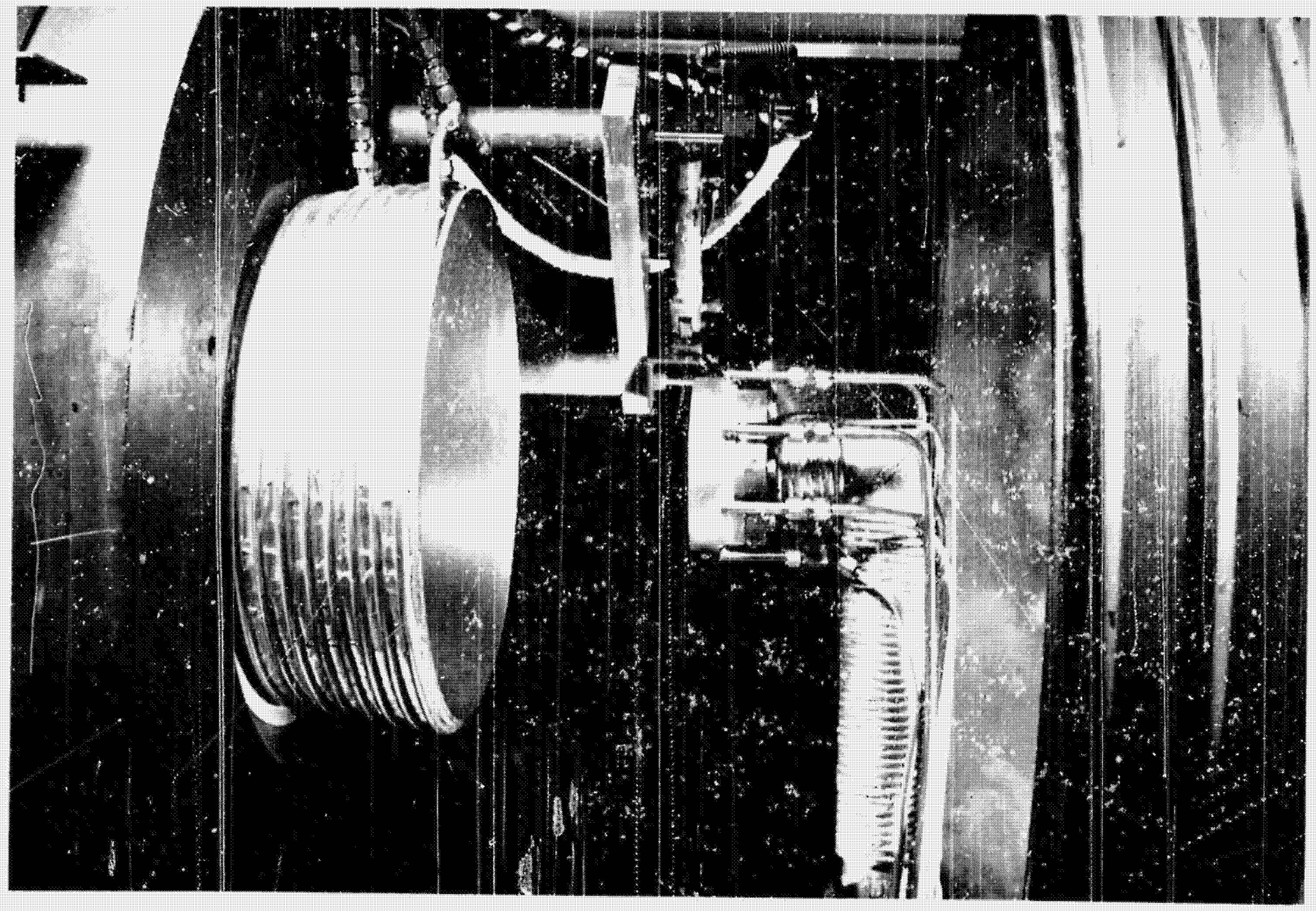

Fig. 3.- Multiple sample support mounted in test chamber.

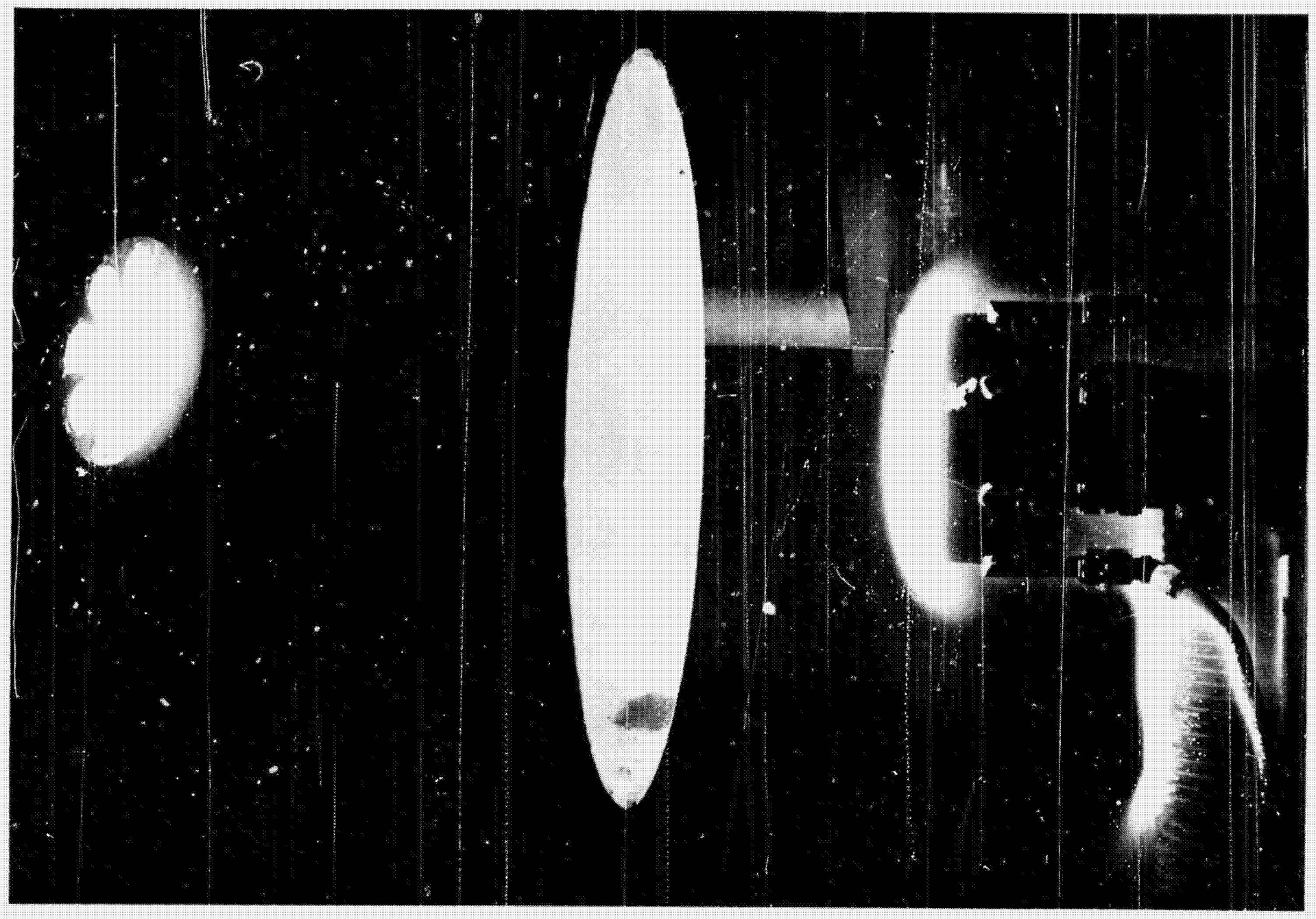

Fig. 4.- Specimens during typical test run.

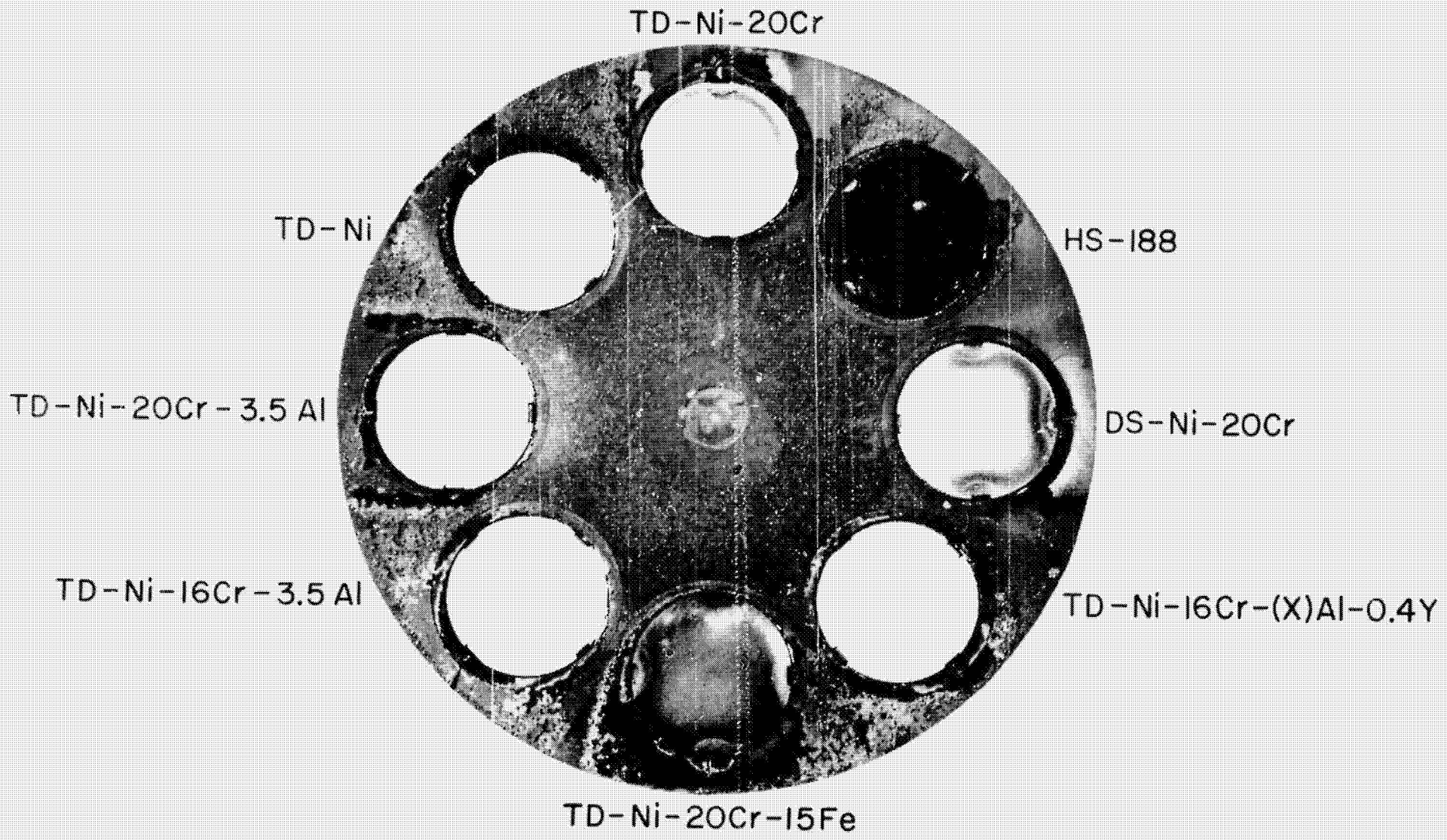

Fig. 5.- Test specimens after 50 cycles of exposure.

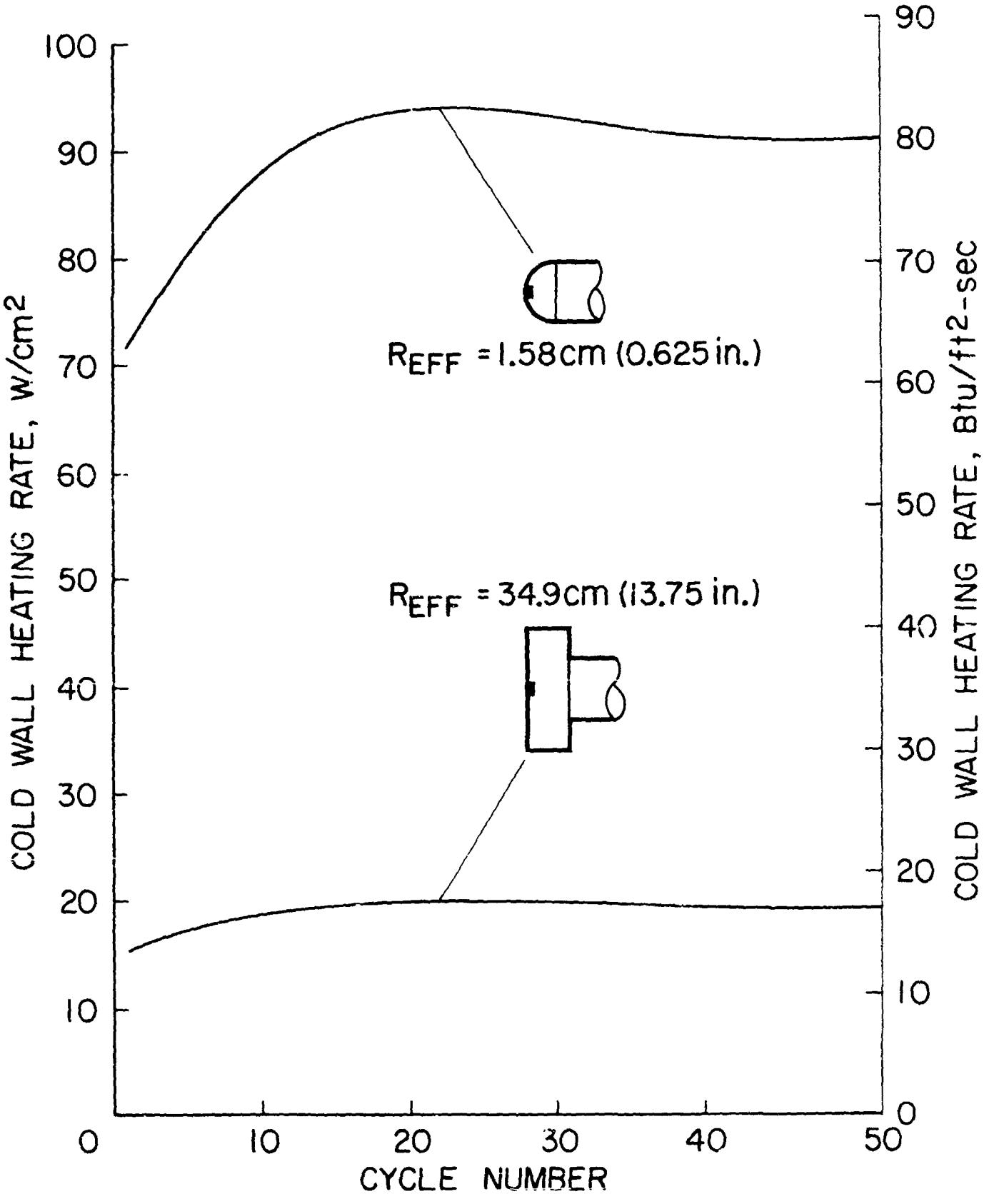

Fig. 6.- Heating rate history.

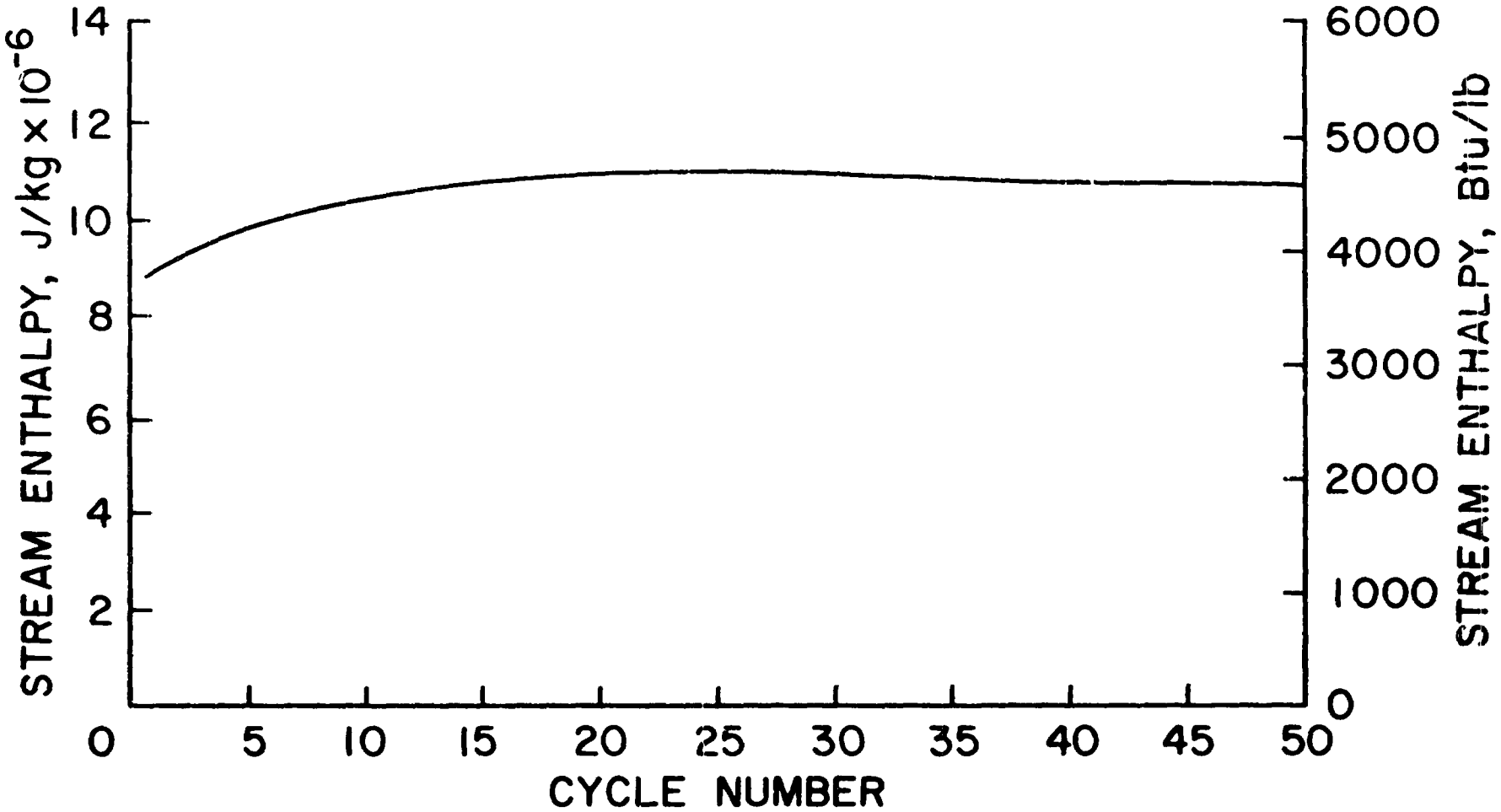

Fig. 7.- Enthalpy history.

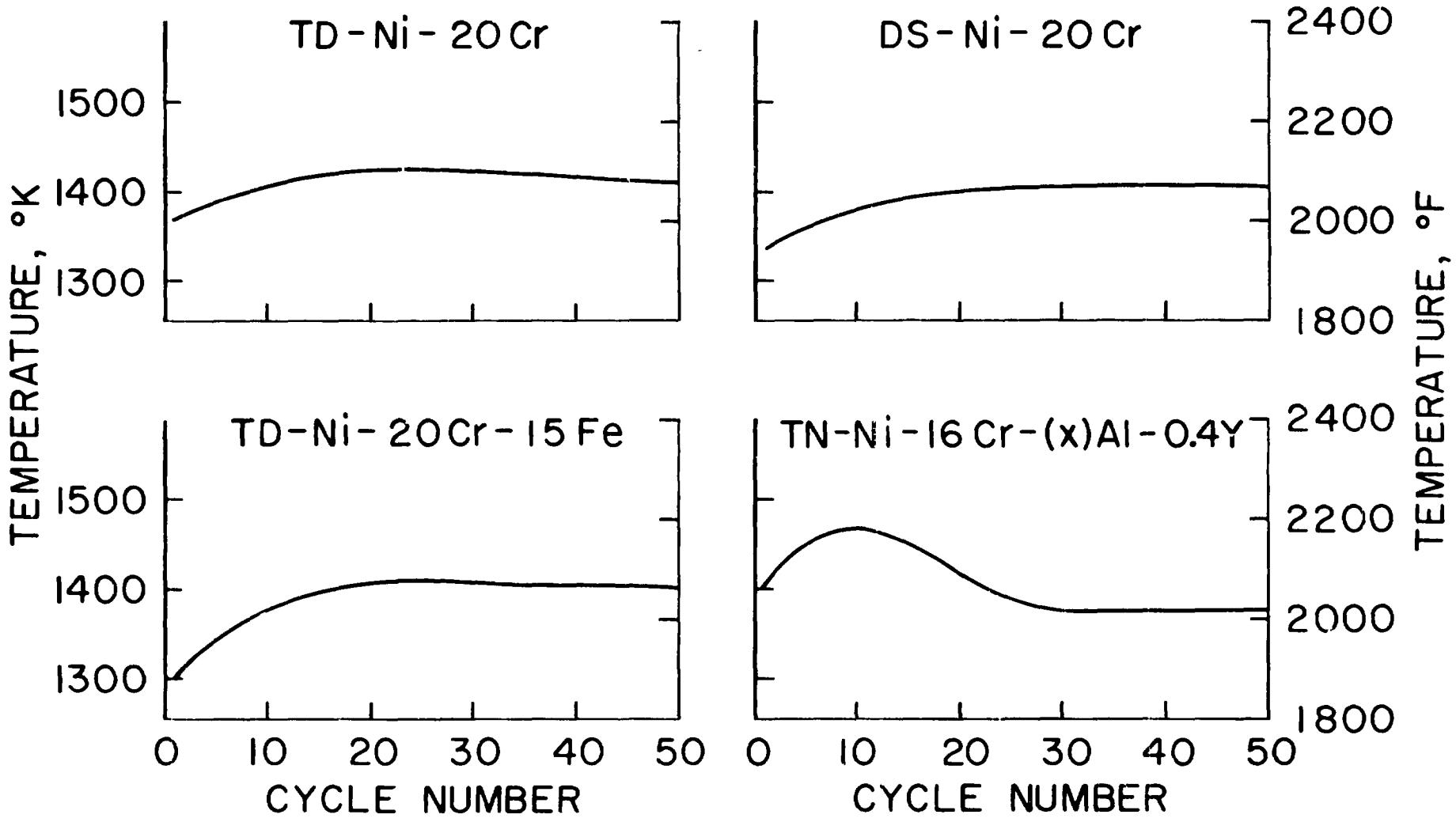

(a) TD-Ni-20Cr;DS-Ni-20Cr;TD-Ni-20Cr-15Fe;TD-Ni-16Cr-(x)Al-0.4Y

Fig. 8.- Temperature histories for the test specimens.

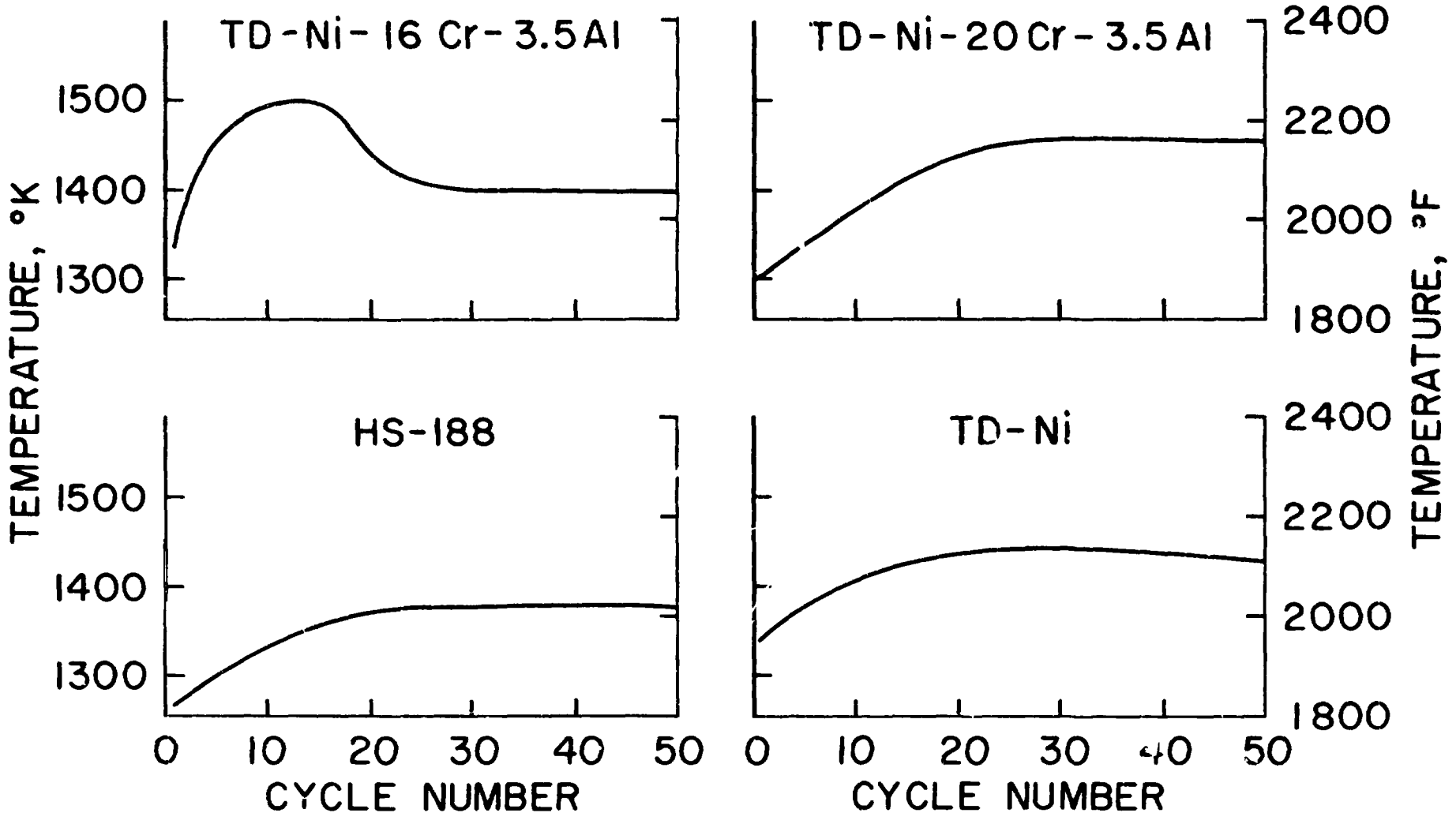

(b) TD-Ni-16Cr-3.5Al;TD-Ni-20Cr-3.5Al;HS-188;TD-Ni

Fig. 8.- Concluded.

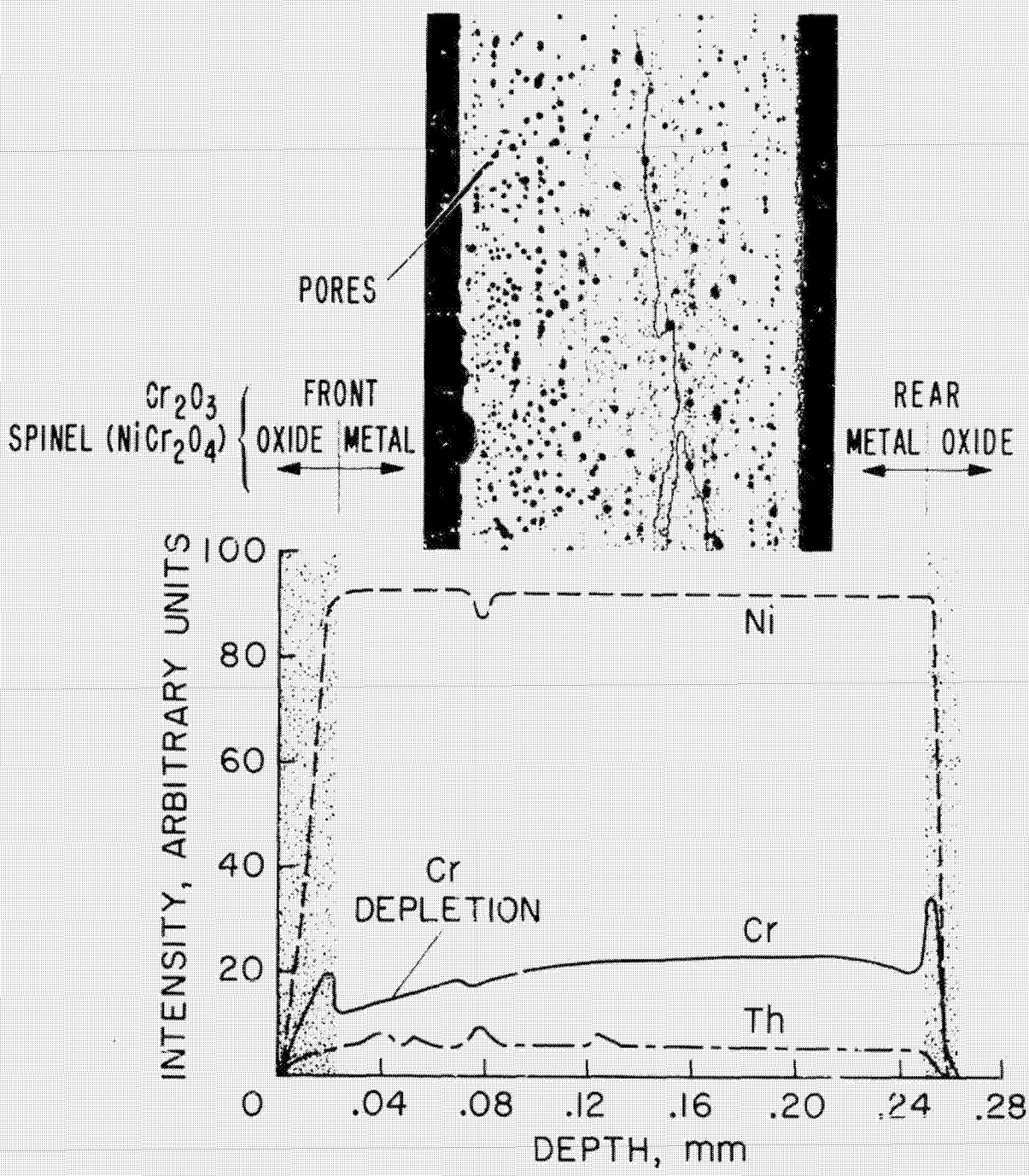

Fig. 9.- Microprobe analysis and microstructure of TD-Ni-20Cr (Lewis Research Center).

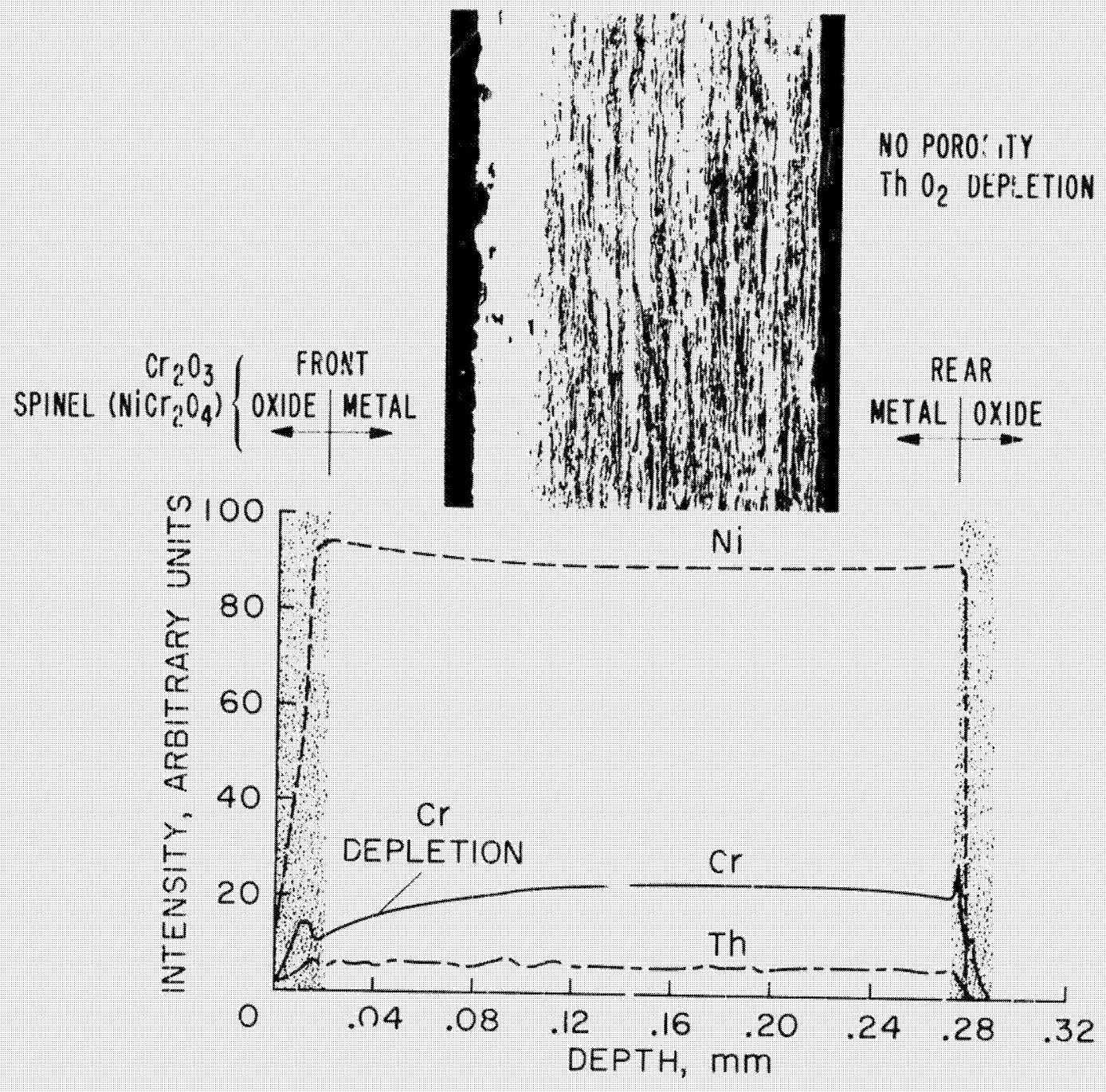

Fig. 10.- Microprobe analysis and microstructure of DS-Ni-20Cr (Lewis Research Center).

Fig. 11.- Electron micrograph of DS-Ni-20Cr; 15,500x (Lewis Research Center).

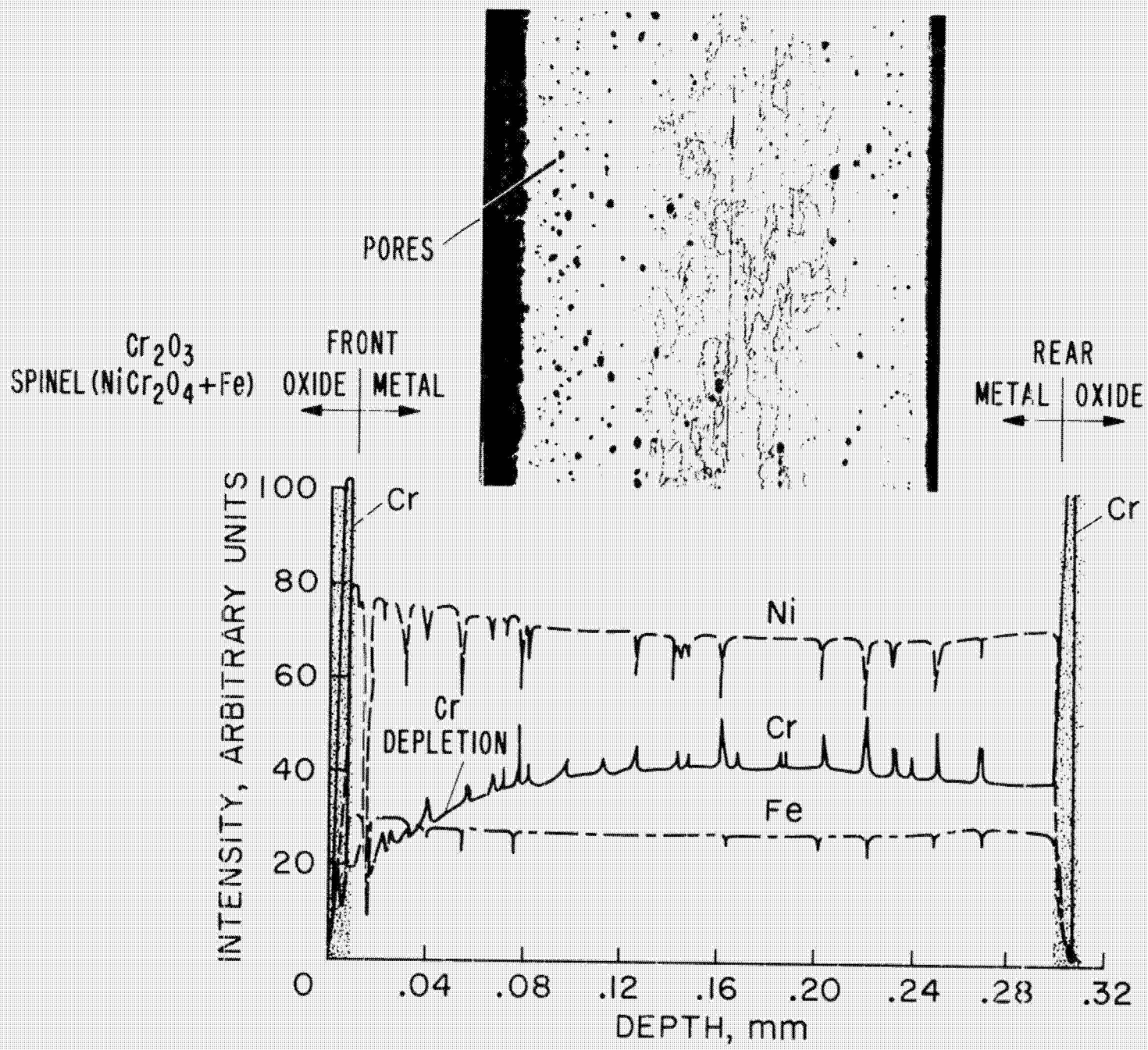

Fig. 12.- Microprobe analysis and microstructure of TD-Ni-20Cr-15Fe (Lewis Research Center).

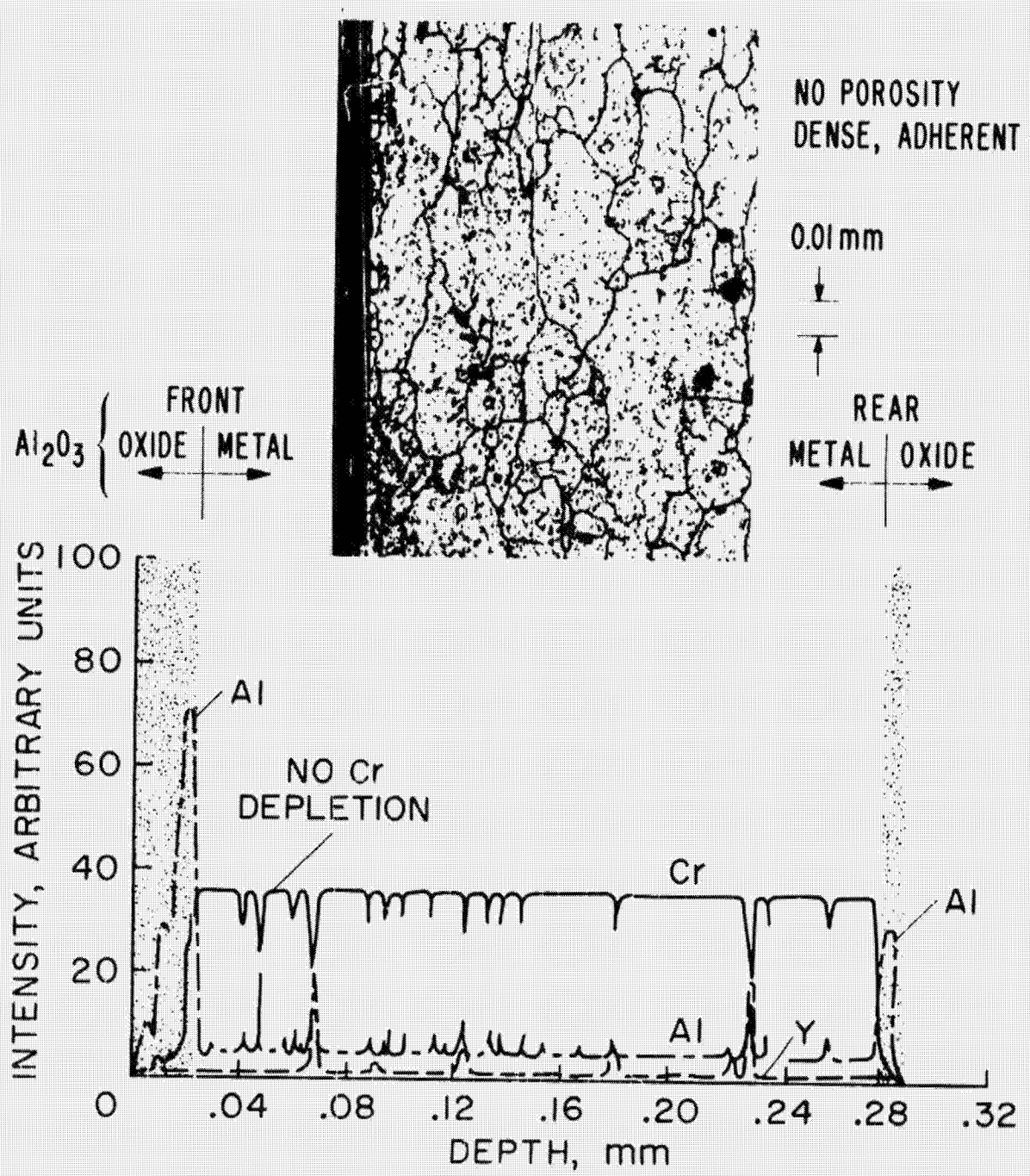

Fig. 13.- Microprobe analysis and microstructure of TD-Ni-16Cr-(x)Al-0.4Y (Lewis Research Center).

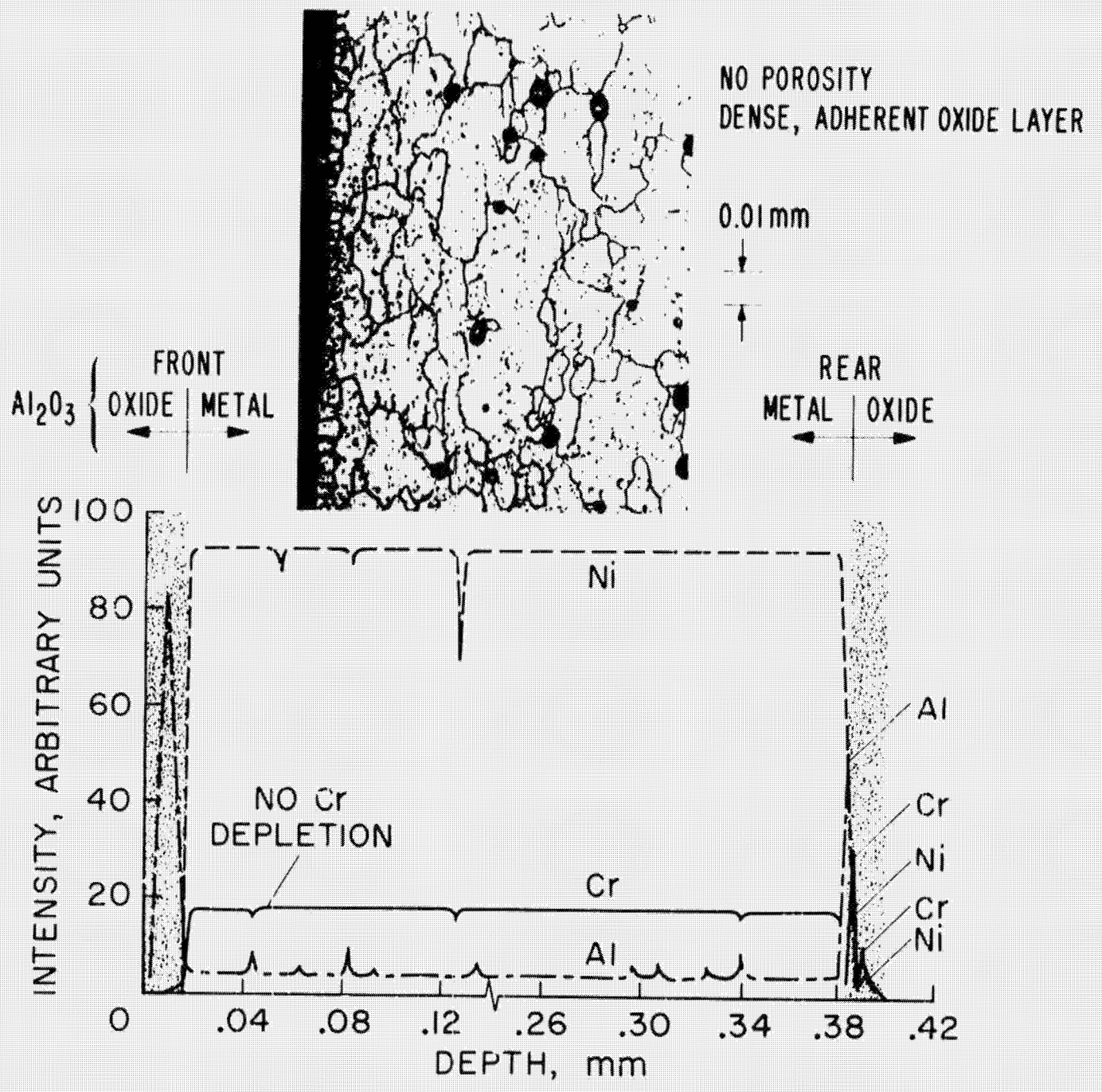

Fig. 14.- Microprobe analysis and microstructure of TD-Ni-16Cr-3.5Al (Lewis Research Center).

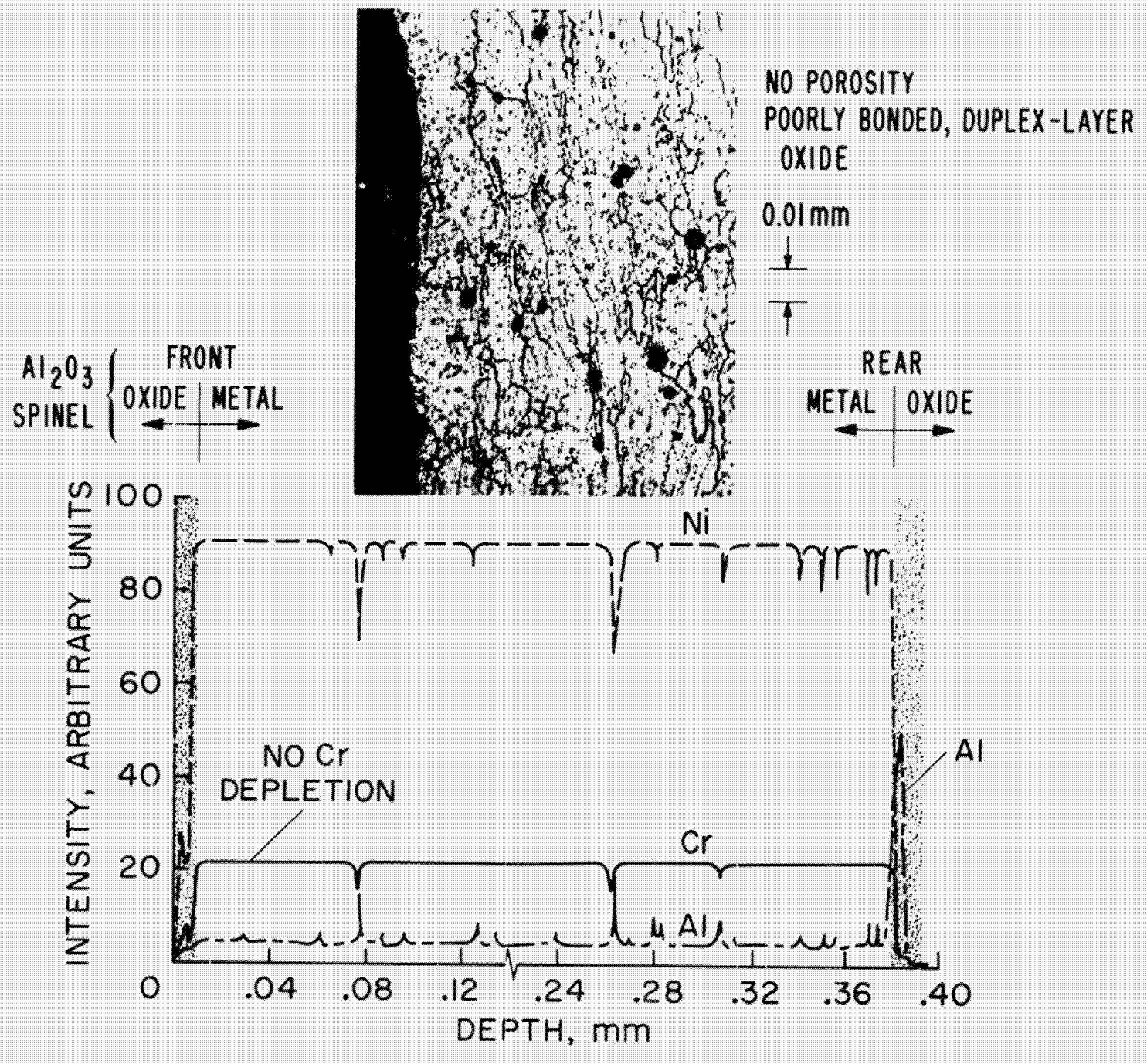

Fig. 15.- Microprobe analysis and microstructure of TD-Ni-20Cr-3.5Al (Lewis Research Center).

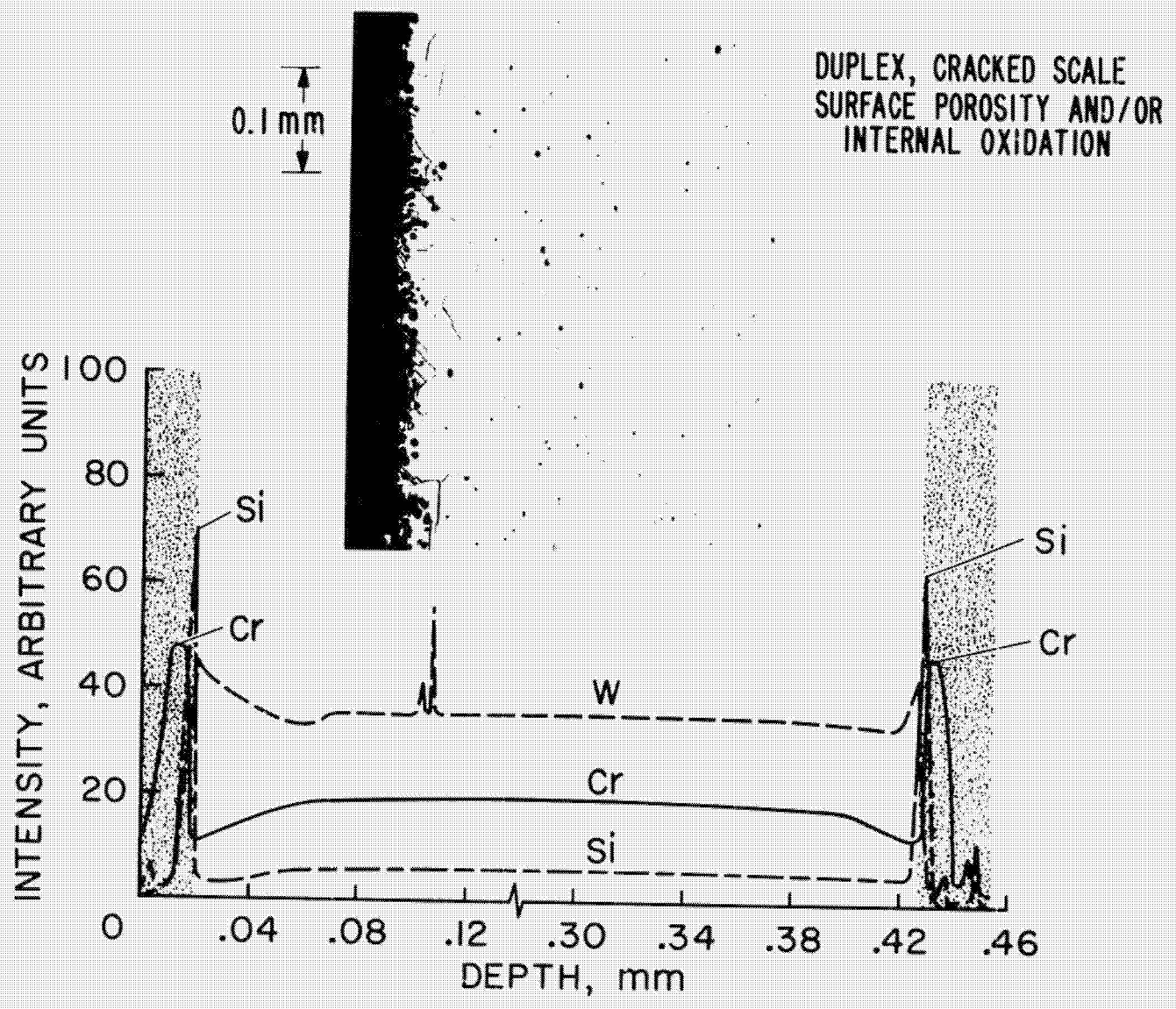

(a) Tungsten, chromium, silicon.

Fig. 16.- Microprobe analysis and microstructure of HS-188 (Lewis Research Center).

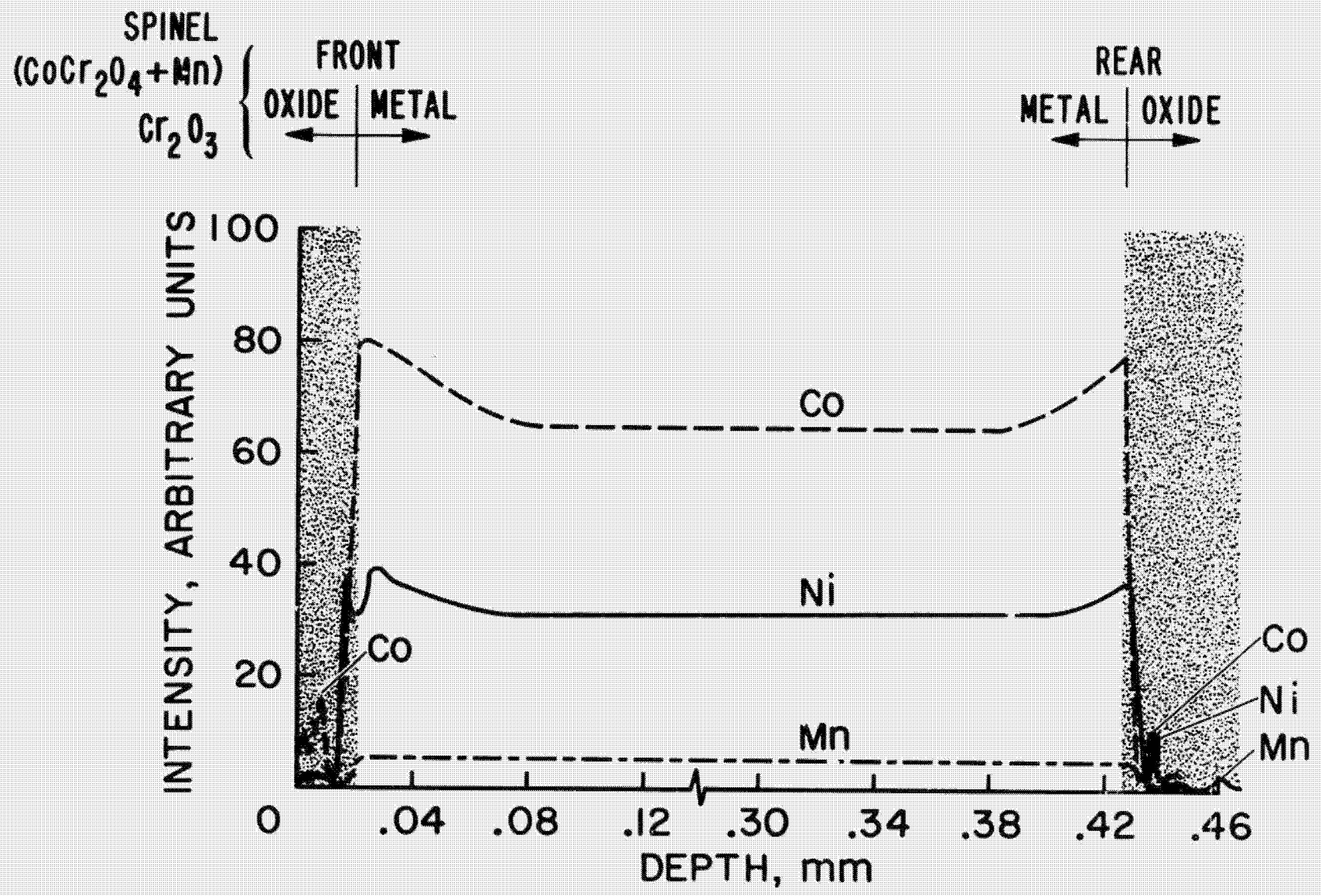

(b) Cobalt, nickel, manganese.

Fig. 16.- Concluded.

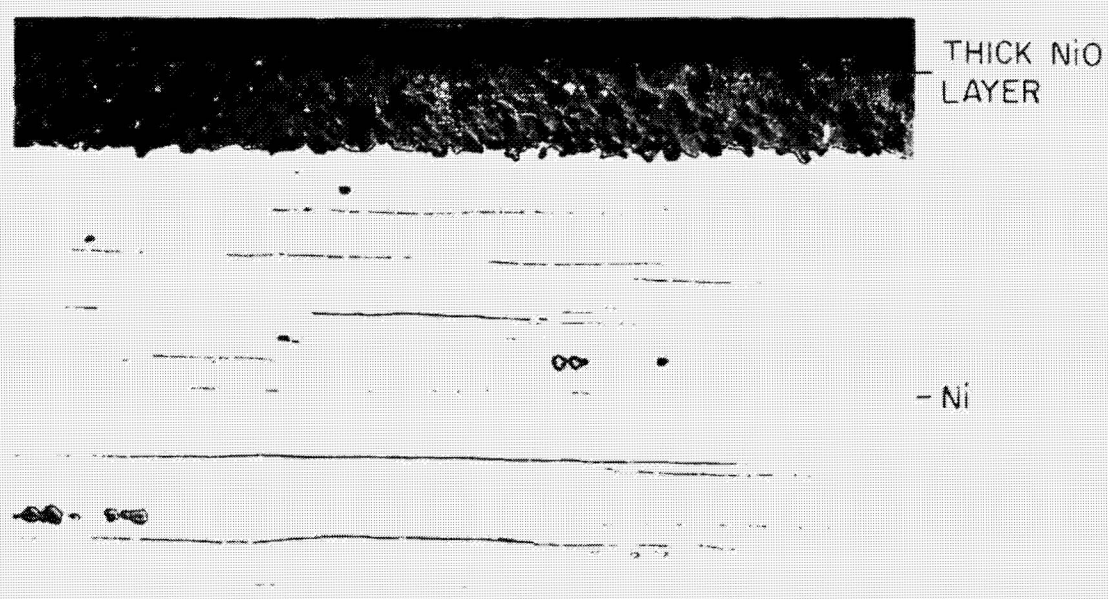

Fig. 17.- Microstructure of TD-Ni (Lewis Research Center).